Chem Rep, 2020, 2(1): 118-123
DOI: 10.25082/CR.2020.01.001

RESEARCH ARTICLE

Controlled growth and waste water treatment of light rare earth (La, Ce, Pr) oxides with 3D superstructures

Lin Li [1] Huimin Ren[1] Bohui Wei[2] Hui Li[2] Chenzhong Yao[1,2*]

Abstract: Light rare earth (La, Ce, Pr) oxides with 3D superstructure are a kind of particularly interesting materials because of their unique optical, electronic, magnetic, and catalytic properties arising from the confinement of the 4f electrons. Here, we report a rapid and simple electrodeposition methodology for the assembly of three-dimensional (3D) superstructures of La_2O_3, CeO_2, and Pr_2O_3 nanobelts using the nitrates based electrolytes with NH_4Ac, and KCl as additives. The removal efficiencies of Congo red solution for La_2O_3, CeO_2, and Pr_2O_3 nano superstructures can reach 68%, 76% and 71% in dark. But CeO_2 show better removal efficiency than La_2O_3 and Pr_2O_3 under light irradiation.

Keywords: light rare earth oxide, superstructure, electrodeposition, waste water treatment

1 Introduction

Recently, nanoscience development has gone beyond the simple pursuit of single nanoparticles, and many efforts have been focused on the assembly of functional nanoscale building blocks, such as nanorods, nanowires or nanotubes, into an appropriate superstructure[1,2]. Once such building blocks can be rationally assembled into appropriate three-dimensional (3D) superstructures, they will offer new scientific opportunities for investigating the influence of size and dimensionality with respect to their collective optical, magnetic, and electronic properties and could provide the possibility to probe novel properties and applications resulting from the spatial orientation and arrangement of the nanocrystals[3–7]. To date, a wide variety of superstructures of inorganic materials, including metals, metal oxides, sulfides, hydrates, and other minerals, have been successfully prepared. However, there has only been limited success in assembling nanobelts into 3D superstructures. It still remains a significant challenge to develop facile methods for the fabrication and architectural control of 3D superstructures[8–10].

The rare-earth oxides (REO) are a particularly interesting class of materials because of their unique optical, electronic, magnetic, and catalytic properties arising from the confinement of the 4f electrons[11–13]. Despite intense experimental efforts, a simple and general route for the preparation of shape-controlled rare earth oxide 3D superstructures has been lacking[1,14–16]. Here we report the development of a rapid, simple, and versatile electrodeposition methodology for the synthesis of 3D nano superstructures of light rare earth oxides (La_2O_3, CeO_2, and Pr_2O_3). To the best our knowledge, this is the first report on a general and rapid method for the synthesis of 3D superstructures of light rare earth oxide. The electrodeposition method is a good candidate for the synthesis of 3D superstructures because of its low cost, rapidity, and potential for large-scale production. The electrodeposition also offers a higher degree of freedom in altering the interplay between the crystal growth rate and the mass transport rate. Also, these kinds of REO show potential application in waste water treatment.

2 Experimental

All reagents used were analytical grade and were used directly without any purification. A simple three-electrode cell was used in our experiments. A Ti foil of about 3.0 cm^2, a graphite rod of about 4.0 cm^2 and a saturated calomel electrode (SCE) were used as the working electrode, counter electrode and reference electrode, respectively. The electrodeposition of La_2O_3/CeO_2/Pr_2O_3 nanobelts was performed in the solution of containing $La(NO_3)_3$/$Ce(NO_3)_3$/$Pr(NO_3)_3$, NH_4Ac, and KCl under

Received: February 13, 2020 **Accepted:** February 28, 2020 **Published:** March 5, 2020

* **Correspondence to**: Chenzhong Yao, School of Chemistry and Materials Science, Shanxi Normal University, Linfen, Shanxi 041004, China & Department of Applied Chemistry, Yuncheng University, Yuncheng, Shanxi 044000, China Email: yaochzh1999@126.com
[1] School of Chemistry and Materials Science, Shanxi Normal University, Linfen, Shanxi 041004, China
[2] Department of Applied Chemistry, Yuncheng University, Yuncheng, Shanxi 044000, China

Citation: Li L, Ren HM, Wei BH, *et al.* Controlled growth and waste water treatment of light rare earth (La, Ce, Pr) oxides with 3D superstructures. *Chem Rep*, 2020, **2**(1): 118-123.

galvanostatic conditions with a cathodic current density at 70°C.

The deposition equipment is a transistor rectifier of auto-control (HDV-7C, Fujian Changlian Electronic Co., Ltd)The obtained deposits were characterized by field emission scanning electron microscope (FE-SEM, JSM-6330F), energy-dispersive X-ray spectroscopy (EDS, FEI/Quanta 400). The isothermal adsorption experiment was carried out in dark and light in a glass reactor with a stirring speed of 500 rpm/min at room temperature. The visible light condition is 500 W Xenon lamp (wavelength: 200-800 nm). Typically, 20 mg of REO samples (powders) were suspended in 100 ml Congo red solution (60 mg/L). Then, at the given time intervals, 3 ml solution samples were collected, filtered by a 0.45 μm film to remove the catalyst. The concentration of the dyes was tested with wavelength of 498 nm by using a Cary5000 UV-Vis-NIR spectrophotometer immediately. For the recycling experiment of La_2O_3 and Pr_2O_3, they were treated under NaOH solution (pH=10) after each recycle.

3 Results and discussion

The electrochemical formation process of the rare earth oxides can be summarized in two main steps. Firstly, the electroreduction of the nitrate or the aerated aqueous solvent, induces an increase of the interfacial concentration of OH^- at the cathode surface (Reaction (1)). Then the OH^- ions produced will result in the formation of rare earth oxides by precipitation Reaction (2 or 3) or Reaction (4) (M=La and Pr; R=Ce)[17, 18].

$$NO_3^- + H_2O + 2e \rightarrow NO_2^- + 2OH^- \quad (1)$$

$$2M\,(III) + 6OH^- \rightarrow M_2O_3 + 3H_2O \quad (2)$$

$$2M\,(III) + 2OH^- + O_2 \rightarrow M_2O_3 + H_2O \quad (3)$$

$$4R\,(III) + 12OH^- + O_2 \rightarrow 4RO_2 + 6H_2O \quad (4)$$

Herein 3D nano-superstructures of light rare earth oxides (La_2O_3, CeO_2, and Pr_2O_3) having various shapes were prepared via electrodeposition (90 min, 70°C) with NH_4Ac and KCl as additives: chloride baths usually increasing coating adhesion[19]. Taking CeO_2 as a representative example, the 3D superstructures were successfully prepared when the electrodeposition was carried out in a solution of 0.01 M $Ce(NO_3)_3$+0.2M NH_4Ac+0.05 M KCl with different current density. Typical SEM images are shown in Figure 1(a, b). The average radius and length are about 40 nm and 2 μm, respectively. The formation of loose and ordered structures is correlative with the H_2 gas bubbles, which move towards the electrolyte/air interface during electrodeposition. Thus, nanorods growth towards the gas bubble will be prohibited, which leads to deposition only occurring between gas bubbles and the formation of porous structures accordingly. When the deposition current is 2 mA·cm^{-2}, lower density nanorod structures were synthesized as shown in Figure 1(c, d, which clearly shows the 3D structures are also composed of nanorods. Figure 2 is EDS results of CeO_2.

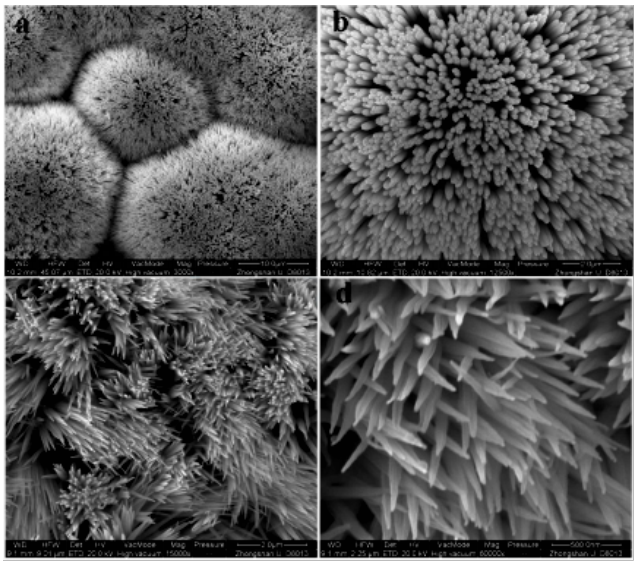

Figure 1. EM images of 3D superstructures of CeO_2 nanorods prepared in solution of 0.01 M $Ce(NO_3)_3$+0.2 M NH_4Ac+0.05 M KCl with different current density. Fig(a, b): 4 mA·cm^{-2}; Fig(c, d): 2 mA·cm^{-2}

When electrodeposition was carried out in a solution containing 0.02 M NH_4Ac, the flower-like porous nanostructures were synthesized. SEM images of the samples are reported in Figure 3(a), which clearly shows that the 3D flower-like structures consist of nanowires. The average diameter of these nanowires is about 50 nm. The pore sizes are about 1 μm. When the electrodeposition current density was shifted to 2 mA·cm^{-2}, lower density flower-like structures were synthesized as shown in Figure 3(b), which clearly shows the 3D flower-like structures are also composed of nanowires.

The La_2O_3 and Pr_2O_3 3D superstructures are also as shown in Figure 4 and Figure 5. With decrease of the current density, the nanobelts of La_2O_3 will become much thinner. The nanobelts have been changed to be bricks with a thickness of 400-600 nm. At 1 mA·cm^{-2}, the SEM of Pr_2O_3 nanorods shows that the densities of the structure can be affected seriously by the current densities. Also, the EDS results of La_2O_3 and Pr_2O_3 are given in Figure 6.

Figure 7 illustrates the whole process of CeO_2 deposit morphology evolution. On this basis, 3D superstructures of other light rare earth oxides, such as La_2O_3 and Pr_2O_3

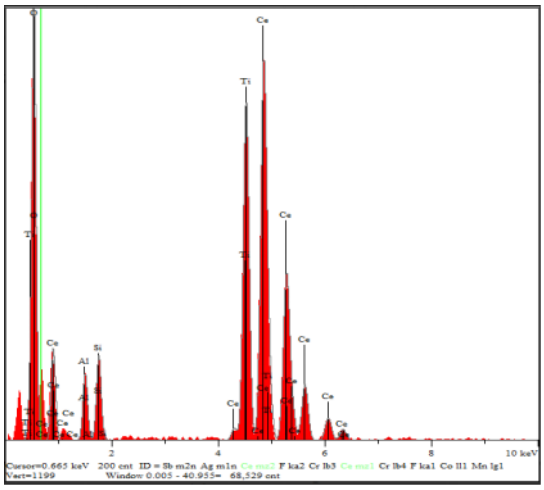

Figure 2. EDS of CeO_2

were also successfully synthesized via electrodeposition by adding NH_4Ac and KCl. In all cases, the concentration of NH_4Ac and deposition current appears to be crucial for the formation of the various 3D superstructures. The formation of rare earth oxide superstructures was previously attributed to the effect of NH_4^+ on the deposition rate through their adsorption on the surfaces of nuclei[20]. Concerning the changes of 3D superstructures, the influence of acetate seems to be preponderant due to the formation of soluble stable complexes, depending on the Ac/M(III) or Ac/R(III) ratio[21]. The greater the level of complexation, the slower the dissociation step and the higher the time allowed to the nucleation and growth phenomena[22]. However, the particular formation of belts on the nanoscale and different 3D superstructures on the mesoscopic scale are as yet not fully elucidated. They could result from preferential kinked surfaces, such as the (III) plane, according to the periodic bond chain (PBC) theory[23]. But other mechanisms are usually required for the formation of needle-like structures with a high aspect ratio: previous studies suggested thus topotactic mechanism in alkaline media[24] or defect-induced growth

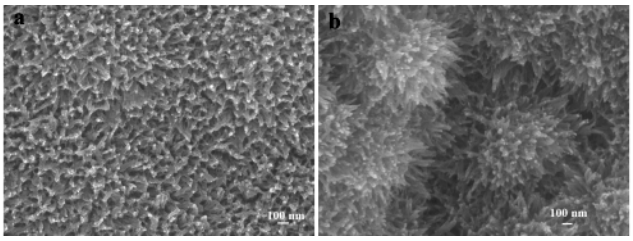

Figure 3. 3D superstructures of CeO_2 were successfully prepared when the electrodeposition was carried out in a solution of 0.01M $Ce(NO_3)_3$+0.02M NH_4Ac+0.05M KCl at 70°C. Fig(a): 4 mA·cm^{-2}; Fig(b): 2 mA·cm^{-2}

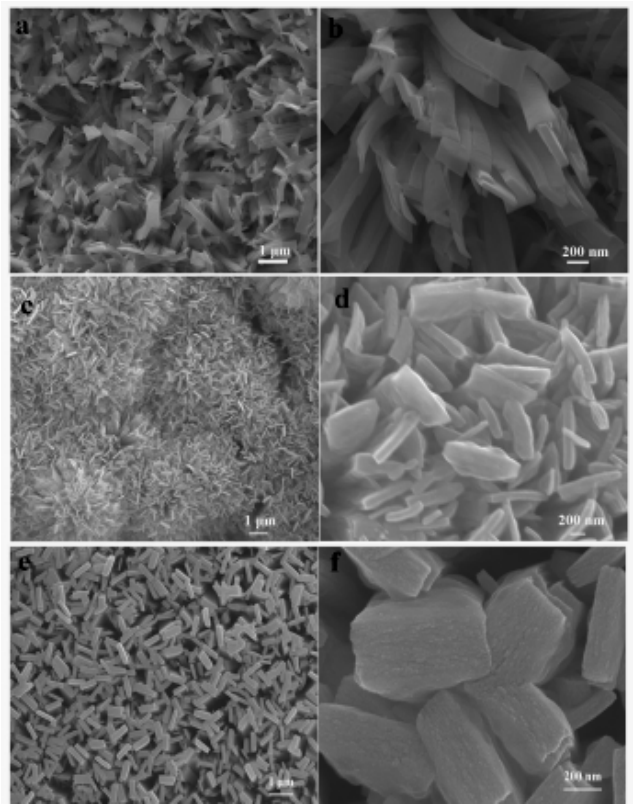

Figure 4. 3D superstructures of La_2O_3 belts were successfully prepared when the electrodeposition was carried out in a solution of 0.01 M $La(NO_3)_3$+0.2 M NH_4Ac+0.05 M KCl at 70°C with different current density. Fig(a, b): 4 mA·cm^{-2}; Fig(c, d): 2 mA·cm^{-2}; Fig(e, f): 1 mA·cm^{-2}

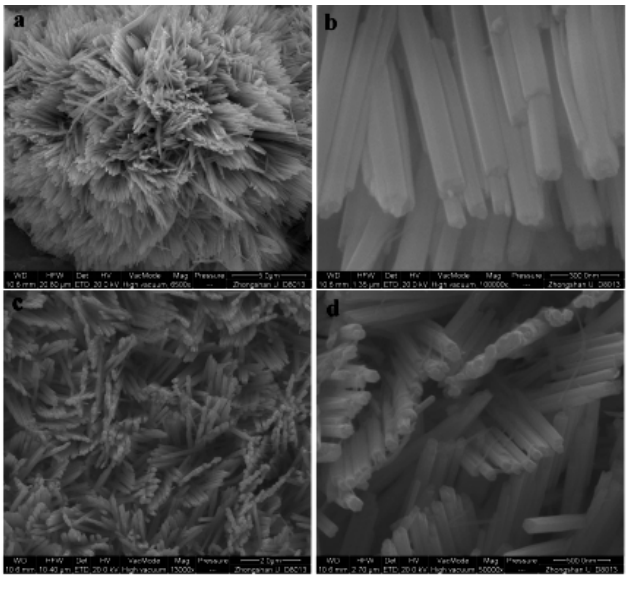

Figure 5. SEM images of 3D superstructures of Pr_2O_3 nanorods prepared in solution of 0.01 M $Pr(NO_3)_3$+0.2 M NH_4Ac+0.05 M KCl with different current density. Fig(a, b): 4 mA·cm^{-2}; Fig(c, d): 2 mA·cm^{-2}

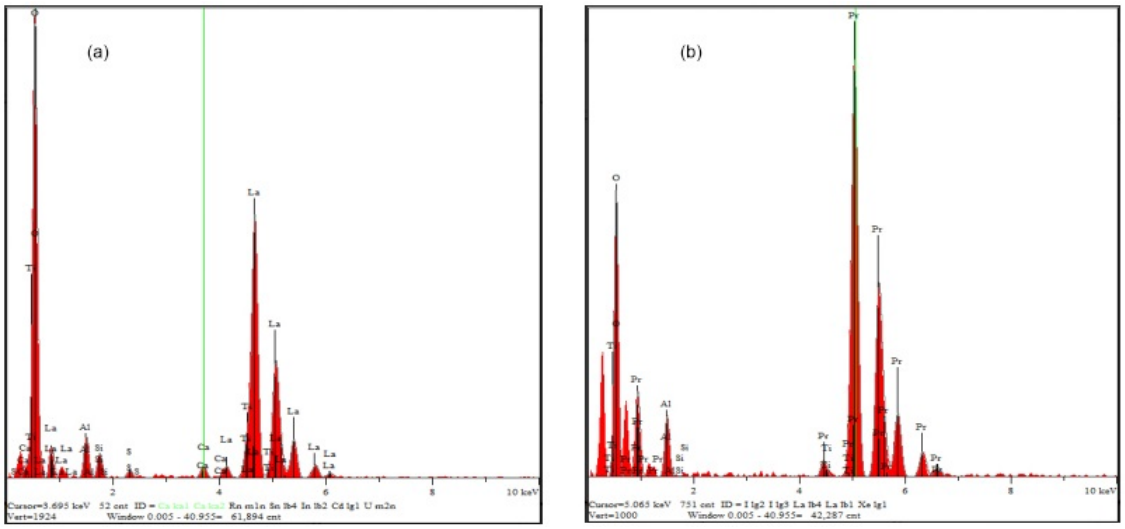

Figure 6. EDS of La_2O_3 and Pr_2O_3

and/or impurity-inhibited growth[23]. From this point of view, NH_4^+ adsorption and/or the remaining small quantity of La(III) impurity and/or the possible incorporation of chloride into the fresh precipitates would be significant.

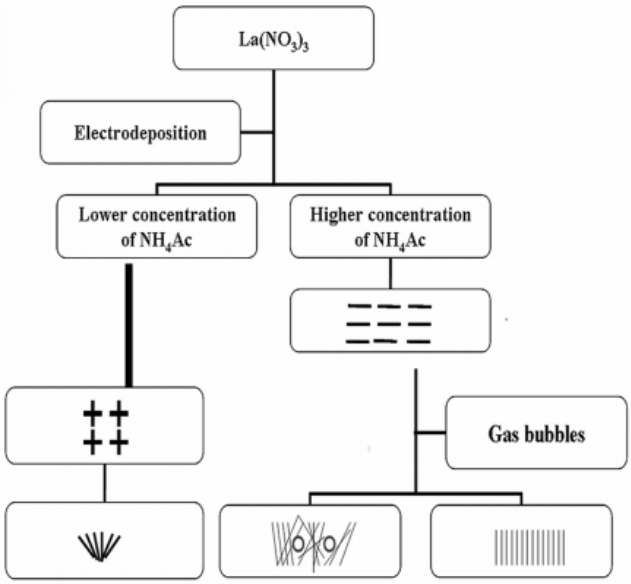

Figure 7. Schematic illustration of the evolution of the whole morphology process

To demonstrate the potential applications in waste water treatment under visible light, the absorption rates of a solution of Congo red in the presence of the resulting samples at different time intervals are shown in Figure 8. The removal efficiencies of Congo red solution for La_2O_3, CeO_2, and Pr_2O_3 nano superstructures reached 68%, 76% and 71% in the first 20 min in dark. With time prolonging, the variation of the removal efficiencies of the three is relatively small (Figure 8(a)). It is worth noting that the visible light has an obvious effect on the removal efficiency of CeO_2, which reached 94.7% in the first 20 min (Figure 8(b)). This may be due to the properties of semiconductor photocatalysts of nano CeO_2[24,25]. The result demonstrates that both catalytic effect and physical absorption of CeO_2 have an effect on the removal of Congo red. Moreover, the CeO_2 nano superstructures have good cycling stability, which exhibits no any decay of their photocatalytic activities after three cycles. But for La_2O_3 and Pr_2O_3 samples, the light condition scarely affects their removal capacities, which are 74% and 77%, respectively (Figure 8(c)). The removal efficiency of 59% and 55% are only retained after three loop operations for La2O3 and Pr_2O_3. This illustrates that the pollution removal is just by physical absorption. This change might be caused by the decrease of the surface area[1].

4 Conclusion

In summary, a general, rapid, and efficient electrodeposition methodology is reported for the first time for the synthesis of various 3D superstructures of REO. This electrodeposition approach has shown great flexibilities in controlling the sizes and shapes of the light rare earth oxides. These novel 3D nano superstructures of light rare earth oxides may bring new opportunities to this established but active field of research. Furthermore, the removal efficiency of Congo red solution for La_2O_3, CeO_2, and Pr_2O_3 nano superstructures reaches 68%, 76% and 71% in dark. But CeO_2 show better removal efficiency than La_2O_3 and Pr_2O_3 under light irradiation. This work not only demonstrates a facile electrochemical method to synthesize REO nano superstructures, but may also open

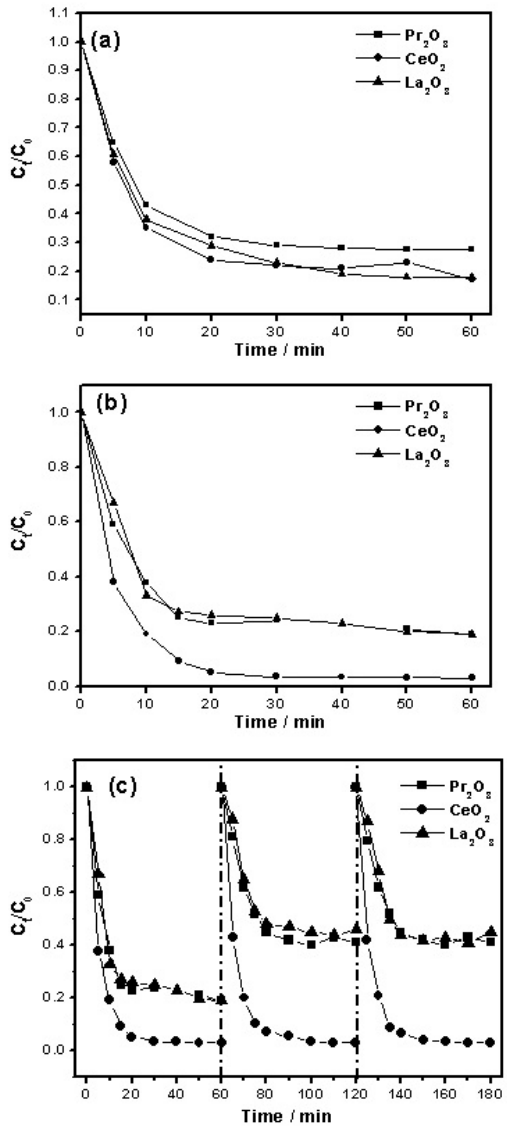

Figure 8. Adsorption rates of Congo red under different conditions: Fig(a): dark light; Fig(b): visible light; Fig(c): cycling stability with visible light

up new opportunities for the design and preparation of highly efficient photocatalysts.

Acknowledgements

This work was supported by the National Natural Science Foundation of China (Nos. U1810110, 21576230 and 51808485), China Scholarship Fund, the Natural Science Foundation of Shanxi (Nos. 201903D121105, 201701D211004 and 201701D221045), the Chemical Key Subject Construction Project of Yuncheng University, the Foundation from Beijing Key Laboratory of plastics health and safety quality evaluation technology (BS201709), and the Foundation from the Key Laboratory of Coal Science and Technology from Taiyuan University of Technology (No. MKX201904).

References

[1] Wei M, Gao L, Li J, *et al*., Activation of peroxymonosulfate by graphitic carbon nitride loadedon activated carbon for organic pollutants degradation. Journal of Hazardous Materials, 2016, **316**: 60-68. https://doi.org/10.1016/j.jhazmat.2016.05.031

[2] Lu XH, Zheng DZ, Zhang P, *et al*. Facile synthesis of free-standing CeO2 nanorods for photoelectrochemical applications. Chemical Communications, 2010, **46**(41): 7721-7723. https://doi.org/10.1039/c0cc01854f

[3] Singh J, Roychoudhury A, Srivastava M, *et al*. A highly efficient rare earth metal oxide nanorods based platform for aflatoxin detection. JJournal of Materials Chemistry, 2013, **1**(35): 4493-4503. https://doi.org/10.1039/c3tb20690d

[4] Yang ML and Song YM. Synthesis and investigation of water-soluble anticoagulant warfarin/ferulic acid grafted rare earth oxide nanoparticle materials, RSC Advances, 2015, **5**(23): 17824-17833. https://doi.org/10.1039/C4RA14633F

[5] Chen HY, Hu J, Zhang J, *et al*. Separation of particles of rare earth oxides by dielectrophoresis, Journal of Materials Science, 2016, **852**: 542-546. https://doi.org/10.4028/www.scientific.net/MSF.852.542

[6] Tsujimoto S, Masui T and Imanaka N. Fundamental aspects of rare earth oxides affecting direct NO decomposition catalysis. European Journal of Organic Chemistry, 2015, **2015**(9): 1524-1528. https://doi.org/10.1002/ejic.201403061

[7] Zhang SB and Yao C. Controllable growth of Ni-La(OH)3 nanotube arrays and their application in wastewater treatment. Materials Letters, 2013, **94**: 143-146. https://doi.org/10.1016/j.matlet.2012.12.040

[8] Gao Y and Tang ZY. Design and application of inorganic nanoparticle superstructures: current status and future challenges. Small, 2011, **7**(15): 2133-2146. https://doi.org/10.1002/smll.201100474

[9] Han D, Song P, Zhang HH, *et al*. Flower-like In2O3 hierarchical nanostructures: synthesis, characterization, and gas sensing properties. RSC Advances, 2014, **4**(91): 50241-50248. https://doi.org/10.1039/C4RA10497H

[10] Li W, Xie SL, Li MY, *et al*. CdS/CeOx heterostructured nanowires for photocatalytic hydrogen production. Journal of Materials Chemistry A, 2013, **1**(13): 4190-4193. https://doi.org/10.1039/c3ta10394c

[11] Azimi G, Dhiman R, Kwo HM, *et al.* Hydrophobicity of rare-earth oxide ceramics. Nature Materials, 2013, **12**: 315-320. https://doi.org/10.1038/nmat3545

[12] Dong B, Cao BS, He YY, *et al*. Temperature sensing and in vivo imaging by molybdenum sensitized visible upconversion luminescence of rare-earth oxides. Advanced Materials, 2012, **24**(15): 1987-1993. https://doi.org/10.1002/adma.201200431

[13] Yuan L, Huang KK, Hou CM, *et al*. Hydrothermal synthesis and magnetic properties of $ReFe_{0.5}Cr_{0.5}O_3$ (RE = La, Tb, Ho, Er, Yb, Lu and Y) perovskite. New Journal of Chemistry, 2014, **38**(3): 1168-1172. https://doi.org/10.1039/c3nj01046e

[14] Si R, Zhang YW, You LP, *et al*. Rare-earth oxide nanopolyhedra, nanoplates, and nanodisks. Angewandte Chemie International Edition, 2005, **44**(21): 3256-3260. https://doi.org/10.1002/anie.200462573

[15] Su LT, Ye J, Karuturi SK, *et al*. High index, reactive facet-controlled synthesis of one-dimensional single crystalline rare earth hydroxide nanobelts. CrystEngComm, 2011, **13**(17): 5367-5373. https://doi.org/10.1039/c1ce05357d

[16] Nguyen TD. From formation mechanisms to synthetic methods toward shape-controlled oxide nanoparticles. Nanoscale, 2013, **5**(20): 9455-9482. https://doi.org/10.1039/c3nr01810e

[17] Arurault L, Daffos B and Sauvage FX. Nanocrystallized ceria-based coatings prepared by electrochemistry on TA6V titanium alloy. Materials Research Bulletin, 2008, **43**(4): 796-805. https://doi.org/10.1016/j.materresbull.2007.07.019

[18] Li GR, Qu DL, Yu XL, *et al*. Microstructural Evolution of CeO_2 from Porous Structures to Clusters of Nanosheet Arrays Assisted by Gas Bubbles via Electrodeposition. Langmuir, 2008, **24**(8): 4254-4259. https://doi.org/10.1021/la7037526

[19] Sivaraman KM, Ergenemana O, Pan S, *et al*. Electrodeposition of cobalt-yttrium hydroxide/oxide nanocomposite films from particle-free aqueous baths containing chloride salts. Electrochimica Acta, 2011, **56**(14): 5142-5150. https://doi.org/10.1016/j.electacta.2011.03.058

[20] Li GR, Qu DL and Tong YX. Facile fabrication of magnetic single-crystalline ceria nanobelts. Electrochemistry Communications, 2008, **10**(1): 80-84. https://doi.org/10.1016/j.elecom.2007.11.003

[21] Golden TD and Wang AQ. Anodic electrodeposition of cerium oxide thin films II. mechanism studies. Journal of The Electrochemical Society, 2003, **150**(9): C621-624. https://doi.org/10.1149/1.1596165

[22] Li FB and Thompson GE. In situ atomic force microscopy studies of the deposition of cerium oxide films on regularly corrugated surfaces. Journal of The Electrochemical Society, 1999, **146**(5): 1809-1815. https://doi.org/10.1149/1.1391848

[23] Cao G. Nanostructures and nanomaterials, Imperial college press, London, U.K. 2004.

[24] Guo CF, Cao S, Zhang J, *et al*. Topotactic transformations of superstructures: from thin films to two-dimensional networks to nested two-dimensional networks. Journal of the American Chemical Society, 2011, **133**(21): 8211-8215. https://doi.org/10.1021/ja111000m

[25] Yao CZ, Li ZP, Wei BH, *et al*. Hydrogenated ceria nanorods and nanobelts for photoelectrochemical application. Journal of Power Sources, 2015, **283**: 478-483. https://doi.org/10.1016/j.jpowsour.2015.02.146

[26] Zhang C, Zhang XY, Wang YC, *et al*. Facile electrochemical synthesis of CeO_2 hierarchical nanorods and nanowires with excellent photocatalytic activities. New Journal of Chemistry, 2014, **38**(6): 2581-2586. https://doi.org/10.1039/C4NJ00214H